A&A 462, L57–L60 (2007)
DOI: 10.1051/0004-6361:20066660

Astronomy & Astrophysics

LETTER TO THE EDITOR

Extensive multiband study of the X-ray rich GRB 050408⋆

A likely off-axis event with an intense energy injection⋆⋆

A. de Ugarte Postigo[1], T. A. Fatkhullin[2], G. Jóhannesson[3], J. Gorosabel[1], V. V. Sokolov[2], A. J. Castro-Tirado[1], Yu. Yu. Balega[2], O. I. Spiridonova[2], M. Jelínek[1], S. Guziy[1,4], D. Pérez-Ramírez[5], J. Hjorth[6], P. Laursen[6], D. Bersier[7], S. B. Pandey[1,8], M. Bremer[9], A. Monfardini[7], K. Y. Huang[10], Y. Urata[11,12], W. H. Ip[10], T. Tamagawa[11], D. Kinoshita[12], T. Mizuno[13], Y. Arai[13], H. Yamagishi[13], T. Soyano[14], F. Usui[15], M. Tashiro[16], K. Abe[16], K. Onda[16], Z. Aslan[17,18], I. Khamitov[17], T. Ozisik[17], U. Kiziloglu[19], I. Bikmaev[20,21], N. Sakhibullin[20,21], R. Burenin[22], M. Pavlinsky[22], R. Sunyaev[22], D. Bhattacharya[23], A. P. Kamble[23], C. H. Ishwara Chandra[24], and S. A. Trushkin[2]

[1] Instituto de Astrofísica de Andalucía (IAA-CSIC), Apartado de Correos 3004, 18080 Granada, Spain
e-mail: deugarte@iaa.es
[2] Special Astrophysical Observatory, Nizhnij Arkhyz, Zelenchokskaya, Karachaevo-Cherkesia, 369167 Russia
[3] Science Institute, University of Iceland, Dunhaga 3, 107 Reykjavík, Iceland
[4] Nikolaev State University, Nikolska 24, 54030, Nikolaev, Ukraine
[5] Dpto. de Física (EPS), Universidad de Jaén, 23071 Jaén, Spain
[6] Dark Cosmology Centre, Niels Bohr Institute, University of Copenhagen, Juliane Maries Vej 30, 2100 Copenhagen, Denmark
[7] Astrophysics Research Inst., Liverpool John Moores Univ., Twelve Quays House, Egerton Wharf, Birkenhead, CH41 1LD, UK
[8] The UCL Mullard Space Science Laboratory, Holmbury St. Mary, Dorking, Surrey, RH5 6NT, UK
[9] Institut de Radio Astronomie Millimétrique (IRAM), 300 rue de la Piscine, 38406 Saint-Martin d'Hères, France
[10] Institute of Astronomy, National Central University, Chung-Li 32054, Taiwan, PR China
[11] Institute for Physics and Chemical Research (RIKEN), Wako, Saitama 351-0198, Japan
[12] Tokyo Institute of Technology, Ookayama, Meguro, Tokyo 152-8550, Japan
[13] Department of Astronomy and Earth Sciences, Tokyo Gakugei University, Koganei, Tokyo 184, Japan
[14] Kiso Observatory, Institute of Astronomy, University of Tokyo, Mitake-mura, Kiso-gun, Nagano 397-0101, Japan
[15] Japan Aerospace Exploration Agency, Institute of Space and Astronautical Science, Sagamihara, Kanagawa 229-8510, Japan
[16] Saitama University, Sakura-ku, Saitama 338-8570, Japan
[17] TÜBITAK National Observatory, Akdeniz Üniversitesi, 07058, Antalya, Turkey
[18] Akdeniz University, Physics Department, 07058 Antalya, Turkey
[19] Middle East Technical University, Physics Department, Inonu Bulvari, Ankara, 06531, Turkey
[20] Departments of Astronomy, Kazan State University, Kremlevskaya Str., 18, Kazan, 420008, Russia
[21] Academy of Sciences of Tatarstan, Bauman Str., 20, Kazan, 420111, Russia
[22] Space Research Institute (IKI), 84/32 Profsoyuznaya, Moscow, 117997, Russia
[23] Raman Research Institute, Bangalore 560 080, India
[24] National Centre for Radio Astrophysics, Ganeshkhind, Pune, 411007, India

Received 30 October 2006 / Accepted 14 December 2006

ABSTRACT

Aims. Understand the shape and implications of the multiband ligth curve of GRB 050408, an X-ray rich (XRR) burst.
Methods. We present a multiband optical light curve, covering the time from the onset of the γ-ray event to several months after, when we only detect the host galaxy. Together with X-ray, millimetre and radio observations we compile what, to our knowledge, is the most complete multiband coverage of an XRR burst afterglow to date.
Results. The optical and X-ray light curve is characterised by an early flattening and an intense bump peaking around 6 days after the burst onset. We explain the former by an off-axis viewed jet, in agreement with the predictions made for XRR by some models, and the latter with an energy injection equivalent in intensity to the initial shock. The analysis of the spectral flux distribution reveals an extinction compatible with a low chemical enrichment surrounding the burst. Together with the detection of an underlying starburst host galaxy we can strengthen the link between XRR and classical long-duration bursts.

Key words. gamma rays: bursts – techniques: photometric

1. Introduction

X-ray flashes (XRFs) where first identified by *Beppo-SAX* (Heise et al. 2001) as those bursts detected by the X-ray camera but not the γ-ray monitor. Later studies based on the larger sample gathered by *HETE-2* (Sakamoto et al. 2005b) gave a more

⋆ Based on observations collected at SAO, La Silla, Roque de los Muchachos, Haleakala, Kitt Peak, Cerro Tololo, TÜBITAK, Kiso, Observatorio de Sierra Nevada, Plateau du Bure, GMRT and RATAN-600.

⋆⋆ Appendices A and B are only available in electronic form at http://www.aanda.org general (and instrument- independent) classification and confirmed the intermediate group of events, the X-ray rich (XRR) class, previously detected by *Ginga* (Yoshida & Murakami 1994) and *Granat*/WATCH (Castro-Tirado et al. 1994). It is now known that long-duration GRBs (LGRBs), XRRs and XRFs share the same isotropic distribution in the sky, the same duration range and similar spectrum, with the main difference of having respectively lower observed spectral peak energy $E_{\rm peak}^{\rm obs}$ in the νF_ν spectrum. They seem to form a continuum and thereby, most of the proposed models have tried to explain them as a unified phenomena (see a summary of the different models in Granot et al. 2005).

GRB 050408 was detected by WXM, SXC, and FREGATE aboard *HETE-2* (Sakamoto et al. 2005a) at 2005 April 08 16:22:50.93 UT (t_0 hereafter). With an observed peak energy of ~20 keV it was classified as an XRR event. The 1.0 m Zeiss and 6.0 m BTA telescopes at the Special Astrophysical Observatory (SAO) in Russia pointed at the position delivered by *HETE-2* through the GCN (GRB Circular Network) and detected the optical afterglow (de Ugarte Postigo et al. 2005a) coincident with the possition of the X-ray afterglow detected by *Swift*/XRT, which began observing 42 min after the burst (Wells et al. 2005). The precise localisation allowed further optical (Covino et al. 2007) and spectroscopic (Berger et al. 2005; Prochaska et al. 2005) observations, this latter ones detemined a redshift of $z = 1.236$.

In Sect. 2 we present the observations and the reduction methods that have been used for the analysis of the data. Section 3 describes the results that have been obtained, including observations of the host galaxy and modelling of the light curve. Section 4 discusses the implications of the analysis of the light curve.

2. Observations and data reduction

For this work we have compiled over 60 photometric measurements in *U, B, V*, *R*c and *I*c bands from 12 telescopes. The images where reduced using standard techniques based on IRAF[1] and JIBARO (de Ugarte Postigo et al. 2005b).

The burst happened during night time in Japan, where a fast follow up was carried out. The very wide field camera, WIDGET was monitoring the field of view of *HETE-2* when the event was reported but detected no optical emission before, during or after the gamma-ray emission down to an unfiltered limiting magnitude of 9.7 (all limits given throughout the paper are 3-σ). The 1.05 m KISO Schmidt telescope pointed to the error box 20 min after the burst but failed to detect the afterglow. Finally, the 1 m LOT telescope observed the field 55 min after the burst, images that later served to confirm the afterglow (Huang et al. 2005b). The discovery of the afterglow was made with the data of the 1.0 m Zeiss and 6.0 m BTA telescopes in Russia (de Ugarte Postigo et al. 2005a), starting 115 min after the burst, when observations became possible from that site.

Further observations were performed from the 1.5 m Russian-Turkish telescope, in TÜBITAK National Observatory, the 4.0 m Blanco telescope in Cerro Tololo, the 4.0 m Mayall telescope in Kitt Peak, the 2.0 m Faulkes Telescope North (FTN) in Haleakala and the 3.5 m Telescopio Nazionale Galileo (TNG) in la Palma. A specially intense multiband campaign was carried out from the 1.54 m Danish telescope in La Silla, where daily observations were obtained during the first 8 days following the burst onset.

Finally, 8 months after the burst, deep observations were made from the 3.5 m telescope at Calar Alto. In these images we detect the host galaxy of the burst in *B* and *R*c bands and impose a limit in *I*c band.

Optical photometric calibration is based on the observation of several standard fields (Landolt 1992) using the 1.54 m Danish telescope at La Silla and the 1.5 m telescope at Sierra Nevada Observatory. From these observations we derive 12 secondary standards of different brightnesses. A log with the observations and the calibration stars are given as online material.

Our dataset is completed with several millimetre and radio limits. 6 epochs of millimetre observations were carried out with the 6-antenna Plateau de Bure interferometer (PdB, Guilloteau et al. 1992). No detection was obtained in either of the 1 mm or 3 mm bands, although a 3-σ signal was found on the phase center in both observing bands on April 18. Careful re-analysis of the data did not reveal these signals as instrumental artifacts. Based on the extreme spectral slope and the non-detection on April 19, we conclude that this result is either due to a statistical fluctuation or an unusual event of interstellar scattering at high galactic latitude, and not due to a source-intrinsic variation. Data calibration was done using the GILDAS software package[2] using MWC349 as primary flux calibrator and 3C 273 as amplitude and phase calibrator. Further observations where obtained 13 days after the burst at 1.28 GHz from GMRT and at 8.4 GHz from RATAN-600.

3. Results

3.1. Light curve

In order to put together all the radio, millimetre, near infrared (nIR), optical and X-ray data available (including data from Foley et al. 2006 and Soderberg 2005a,b), we have determined the corresponding flux density values for all observations. X-ray afterglow counts, obtained from Foley et al. (2006) have been converted and corrected for hydrogen column extinction using WEBPIMMS[3] taking as spectral model a powerlaw with a slope of $\beta_{\rm X} = 1.16$ and a column density of $N_{\rm H} = 0.25 \times 10^{22}$ cm^{-1} (Nousek et al. 2006; Chincarini et al. 2005). The optical data have been corrected for galactic reddening (using an $E(B-V) = 0.026$, Schlegel et al. 1998) and intrinsic extinction (see Sect. 3.2). The measured/estimated host galaxy flux has been subtracted from the data to obtain the clean afterglow flux (see Sect. 3.3). The conversion of the optical data to flux density was done using the transformations given by Fukugita et al. (1995) for the optical and by Allen et al. (2000) for the nIR. The resulting light curves are shown in Fig. 1. Note the intense bump, rising at ~3 days and peaking at ~6 days, both in optical and X-rays. These kind of fluctuations have already been detected in the light curves of LGRBs and short-duration bursts (SGRBs) (de Ugarte Postigo et al. 2005c, 2006).

3.2. Study of the optical-nIR SFD

We have constructed the *UBVR*c*I*c*JHK*-band Spectral Flux distribution (SFD) of the afterglow 0.6 days after the burst, when near simultaneous optical and nIR observations were available.

[1] IRAF is distributed by the National Optical Astronomy Observatories, which is operated by the Association of Universities for Research in Astronomy, Inc. (AURA) under cooperative agreement with the National Science Foundation.

[2] GILDAS is the software package distributed by the IRAM Grenoble GILDAS group.

[3] `http://heasarc.nasa.gov/Tools/w3pimms.html`

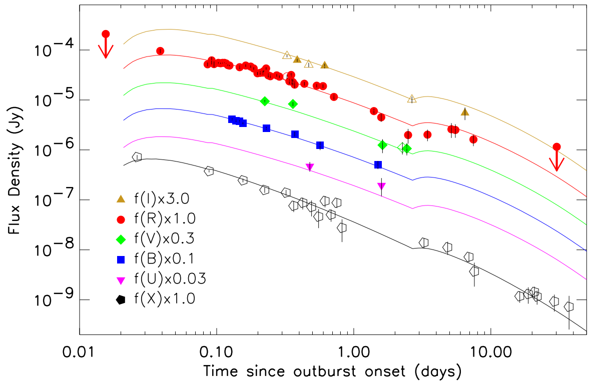

Fig. 1. Multiwavelength light curve of the GRB 050408 afterglow in the observer frame. The lines show the best fit of a fireball model with one energy injection (at 2.9 days) seen off-axis (see text for details). Our observations are plotted with filled symbols, while the ones obtained from the literature are represented by empty ones, this convention is used for all the figures.

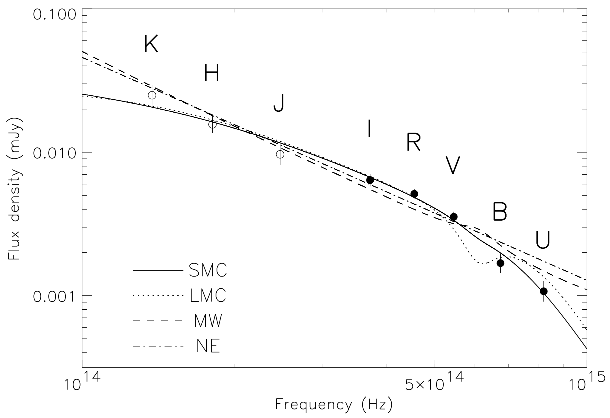

Fig. 2. Spectral flux distribution of the afterglow 0.6 days after the burst onset in the observer frame. The different lines represent results from fitting the data to various extinction laws: Small Magellanic Cloud (SMC), Large Magellanic Cloud (LMC), Milky Way (MW) and No Extinction (NE).

The *UBVRcIc*-band magnitudes from this work were complemented with the *JHK*-band values reported by Foley et al. (2006). Synchronisation to a unique timing is done by assuming a powerlaw with an index of $\alpha = 0.7$ ($F \propto t^{-\alpha}$), as derived from a linear fit of the nearby multiband data of the afterglow.

The fluxes are used for fitting an extincted powerlaw ($F_\nu \propto 10^{-0.4A_\nu}\nu^{-\beta}$) with 3 different extinction laws: Milky Way (MW), Large Magellanic Cloud (LMC) and Small Magellanic Cloud (SMC) as described by Pei (1992). This allows us to obtain A_V and β simultaneously. The results of these 3 fits are complemented with an unextincted powerlaw case (NE), see Fig. 2 and Table 1. The best fit to the SFD of the afterglow is obtained when considering a SMC extinction law (χ^2/d.o.f. = 5.0/5). This is consistent with what has been previously found for other LGRB afterglows (Kann et al. 2006).

3.3. The host galaxy

Several months after the gamma-ray event we revisited the GRB field with the 3.5 m telescope at Calar Alto Observatory in order to search for the host galaxy. Images were obtained in *B*, *Rc* and *Ic* bands, yielding a faint detection in *B* and *Rc*

Table 1. Results of the SFD fitting at 0.6 days for different extinction laws.

Extinction law	β	A_V	χ^2/d.o.f.
MW	1.85 ± 0.30	–0.18 ± 0.22	24.5/5
LMC	–0.12 ± 0.48	1.19 ± 0.32	11.5/5
SMC	0.28 ± 0.33	0.73 ± 0.18	5.0/5
NE	1.62 ± 0.07	0	21.0/5

and imposing a limit on *Ic*. We derive galaxy colour indices of $(B - Rc) = 0.7 \pm 0.5$ and $(Rc - Ic) \leq 0.73$. These values are corrected for Galactic extinction. We have compared these values to the ones derived from the templates computed by Kinney et al. (1996) for a wide variety of galaxy types. We may conclude that only starburst galaxy templates are consistent with them. The best correlation is obtained with the starbust 2 template, with an intrinsic extinction of $E(B - V) = 0.16$.

3.4. Modelling of the multiband data

Using the model and methods described by Jóhannesson et al. (2006) we fitted the multiband observations of the afterglow (galaxy subtracted) to a fireball model with energy injections, viewed both on-axis and off-axis (with varying viewing angles). At least one injection is needed in order to account for the bump seen at 6 days which would carry as much energy as the initial shock. Another characteristic of the light curve is a flattening of the early light curve, seen in Rc and X-rays during the first hours of the burst, which has already been reported by Foley et al. (2006). This can be explained either by an early energy injection (single or continous), or an outflow with a low initial Lorentz factor, or as the result of an off-axis viewed burst. Similar early behaviour has already been found in other bursts (Nousek et al. 2006; Zhang et al. 2006).

Our preferred scenario (giving the best fit) describes the burst as a collimated ($\theta_0 = 2.7°$) fireball seen off axis ($\theta_v = 1.45\theta_0$) expanding into a uniform low density environment ($n_0 = 0.01$ cm^{-3}) with an electron index $p = 2.03$ and having an additional energy injection after 2.9 days with 1.2 times the initial energy. No further injections are needed to explain the light curve with the available amount of data. From the fit we obtain a χ^2/d.o.f. = 158.1/93. The jet break, as defined by Sari et al. (1999), would be expected initially at 1.6 days, or at 3.8 days due to the energy injection. However, due to the effect of the equal arrival time surface, it is further delayed to approximatelly 30 days. Figure 3 shows the radio to X-ray SFD predicted by our model for 3 epochs, together with observational data, host subtraced and corrected for galactic and intrinsic extinction.

4. Discussion

The optical-nIR SFD shows a clear curvature, implying a need for extinction along the afterglow line of sight in the host galaxy. The only reliable fit (χ/d.o.f. = 5.0/5) is based on a SMC extinction law. This result points towards a low stage of chemical enrichment in the region of the progenitor, as is usually found for LGRBs (Kann et al. 2006). The detection of a starburst host galaxy is also a common feature with most LGRBs (Fruchter et al. 2006), facts that once again favour the hypothesis of shared nature between XRR bursts and LGRBs.

The optical spectral index obtained from this fit ($\beta_o = 0.28 \pm 0.33$) and the X-ray one ($\beta_X = 1.14 \pm 0.19$, Nousek et al. 2006) are consistent with a synchrotron spectra in which the cooling

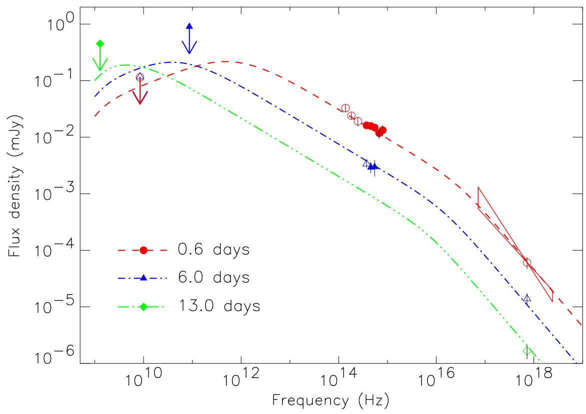

Fig. 3. Spectral Flux Distribution of the afterglow from radio to X-rays 0.6, 6.0 and 13.0 days after the burst in the observer frame. Several 3-σ upper limits from radio and millimetre observations are plotted.

break frequency (ν_c) is located between optical and X-rays. A linear fit of the optical (Rc) and X-ray data between 0.1 and 1.0 days (where there is more data available and the light curve seems more stable) returns temporal slope values of $\alpha_o = 0.69 \pm 0.04$ and $\alpha_X = 0.99 \pm 0.21$. These numbers, together with the optical and X-ray spectral slopes, are consistent with a standard fireball model (Sari et al. 1999) in which a relativistic outflow is expanding in a uniform density environment in the slow cooling regime with an electron power law distribution index of $p \sim 2.0$.

A more complex multirange model, confirms these results and is used to account for the bump that has been detected to peak at ~6 days by allowing for refreshed shocks. This fluctuation is simultaneously observed in optical and X-rays and can be explained by an energy injection of the order of the initial shock. This achromaticity and the simultaneity at both sides of ν_c rules out other explanations such as a density fluctuation, a dust echo or a supernova bump (which could also be ruled out by amplitude and onset time). Other explanations involving an refreshed energy release such as a double jet (Berger et al. 2003) or a patchy shell (Meszaros et al. 1998) can not be discarded. This injection delays the break, that would be expected for about 1.6 days, to about 30 days and, mainly due to the effect of the equal arrival time surface, transforms it to a very smooth break that expands over a decade in time.

To explain the flattening seen in the earliest points of the light curve we have studied the case of a collimated fireball seen off-axis, as predicted by some unified models (Yamazaki et al. 2002) that simultaneously intend to explain LGRBs, XRR bursts and XRFs by only varying the viewing angle. Our fit accounts reasonably well for the multiband and long scale behaviour of the light curve. However, the fits obtained with an on-axis model with an additional early injection or a low initial gamma factor (dirty fireball) can also interpret the data (although returning worse fits) and can not be ruled out.

Regarding the energetics of the afterglow we find that, with an observed peak energy of ~20 keV and a fluence of $\sim 3.3 \times 10^{-6}$ erg cm^{-2} (2–400 keV) it has an isotropic equivalent energy release in γ-rays $E_{\gamma,\mathrm{iso}} \gtrsim 1.3 \times 10^{52}$ erg, at least 6 times greater than the predicted by $E_{\mathrm{peak}} - E_{\mathrm{iso}}$ relation (Amati 2006).

We encourage polarimetric observations of XRR bursts and XRF events (i.e. Gorosabel et al. 2006) as they will be extremely useful to better understand the physics and geometry of the emission and to discriminate between energy models when explaining the fluctuations seen in the light curves.

Acknowledgements. We acknowledge the generous allocation of observing time by different Time Allocation Committees. This work was partially supported by the Spanish MCyT under programmes AYA2004-01515 and ESP2005-07714-C03-03 (including FEDER funds), RFBR grants 04-02-16300 and 05-02-17744 and grant NSh-784.2006.2. The Dark Cosmology Centre is supported by the Danish National Research Foundation. A.d.U.P. acknowledges support from FPU grant AP2002-0446 from the Spanish MCyT. G.J. acknowledges support from the Icelandic Research Council.

References

Allen, C. W. 2000, Astrophysical Quantities, 4th Ed. (London: Athlone)
Amati, L. 2006, MNRAS, 372, 233
Berger, E., Kulkarni, S. R., Pooley, G., et al. 2003, Nature, 426, 154
Berger, E., Gladders, M., & Oemler, G. 2005, GRB Coordinates Network, 3201
Castro-Tirado, A. J., Brandt, S., Lund, N., et al. 1994, Gamma-Ray Bursts, AIP Conf. Proc., 307, 17
Capalbi, M., Malesani, D., Perri, M., et al. 2006, A&A, in press [arXiv:astro-ph/0610845]
Covino, et al. 2007, submitted
Chincarini, G., Moretti, A., Romano, P., et al. 2005 [arXiv:astro-ph/0506453]
Foley, R. J., Perley, D. A., Pooley, D., et al. 2006, ApJ, 645, 450
Fruchter, A. S., Levan, A. J., Strolger, L., et al. 2006, Nature, 441, 463
Fukugita, M., Shimasaku, K., & Ichikawa, T. 1995, PASP, 107, 945
Gorosabel, J., Larionov, V., Castro-Tirado, A. J., et al. 2006, A&A, 459, L33
Guilloteau, S., Delannoy, J., Downes, D., et al. 1992, A&A, 262, 624
Granot, J., Ramirez-Ruiz, E., & Perna, R. 2005, ApJ, 630, 1003
Huang, K. Y., Ip, W. H., Kinoshita, D., et al. 2005b, GRB Coordinates Network, 3196
Heise, J., in't Zand, J., Kippen, R. M., & Woods, P. M. 2001, Gamma-ray Bursts in the Afterglow Era, 16
Jóhannesson, G., Björnsson, G., & Gudmundsson, E. H. 2006, ApJ, 647, 1238
Kann, D. A., Klose, S., & Zeh, A. 2006, ApJ, 641, 993
Kinney, A. L., Calzetti, D., Bohlin, R. C., et al. 1996, ApJ, 467, 38
Landolt, A. U. 1992, AJ, 104, 340
Meszaros, P., Rees, M. J., & Wijers, R. A. M. J. 1998, ApJ, 499, 301
Nousek, J. A., Kouveliotou, C., Grupe, D., et al. 2006, ApJ, 642, 389
Pei, Y. C. 1992, ApJ, 395, 130
Prochaska, J. X., Bloom, J. S., Chen, H.-W., Foley, R. J., & Roth, K. 2005, GRB Coordinates Network, 3204
Reichart, D. E. 2001, ApJ, 554, 643
Sakamoto, T., Ricker, G., Atteia, J.-L., et al. 2005a, GRB Coordinates Network, 3189
Sakamoto, T., Lamb, D. Q., Kawai, N., et al. 2005b, ApJ, 629, 311
Sari, R., Piran, T., & Halpern, J. P. 1999, ApJ, 519, L17
Schlegel, D. J., Finkbeiner, D. P., & Davis, M. 1998, ApJ, 500, 525
Soderberg, A. M. 2005a, GRB Coordinates Network, 3210
Soderberg, A. M. 2005b, GRB Coordinates Network, 3234
Stanek, K. Z., Garnavich, P. M., Nutzman, P. A., et al. 2005, ApJ, 626, L5
de Ugarte Postigo, A., Komorova, V., Fathkullin, T., et al. 2005a, GRB Coordinates Network, 3192
de Ugarte Postigo, A., et al. 2005b, JIBARO: Un conjunto de utilidades para la reducción y análisis automatizado de imágenes, in Astrofísica Robótica en España, ed. A. J. Castro-Tirado, B. A. de la Morena, & J. Torres, Madrid, 35
de Ugarte Postigo, A., Castro-Tirado, A. J., Gorosabel, J., et al. 2005c, A&A, 443, 841
de Ugarte Postigo, A., Castro-Tirado, A. J., Guziy, S., et al. 2006, ApJ, 648, L83
Wells, A. A., Abbey, A. F., Osborne, J. P., et al. 2005, GRB Coordinates Network, 3191
Yamazaki, R., Ioka, K., & Nakamura, T. 2002, ApJ, 571, L31
Yoshida, A., & Murakami, T. 1994, Gamma-Ray Bursts, AIP Conf. Proc., 307, 333
Zhang, B., Fan, Y. Z., Dyks, J., et al. 2006, ApJ, 642, 354

Online Material

Appendix A: Calibration stars

Table A.1. Calibration stars in the field of GRB 050408, as marked in Fig. A.1.

#	RA (J2000)	Dec (J2000)	*U*	*B*	*V*	*R*	*I*
1	12:02:09.16	+10:49:24.1	19.114 ± 0.053	19.174 ± 0.024	18.601 ± 0.009	18.213 ± 0.008	17.835 ± 0.024
2	12:02:10.38	+10:51:37.3	18.982 ± 0.053	19.241 ± 0.024	18.776 ± 0.009	18.438 ± 0.008	18.062 ± 0.025
3	12:02:08.70	+10:51:52.4	19.743 ± 0.054	18.759 ± 0.023	17.167 ± 0.008	16.125 ± 0.007	14.776 ± 0.022
4	12:02:14.68	+10:54.02.8	18.200 ± 0.051	18.508 ± 0.023	18.028 ± 0.008	17.671 ± 0.007	17.292 ± 0.023
5	12:02:11.76	+10:54:59.6	18.204 ± 0.051	17.855 ± 0.023	17.089 ± 0.008	16.627 ± 0.007	16.218 ± 0.022
6	12:02:22.95	+10:53:57.8	18.896 ± 0.051	19.098 ± 0.023	18.638 ± 0.009	18.300 ± 0.008	17.980 ± 0.024
7	12:02:25.20	+10:51:43.6	20.034 ± 0.058	19.143 ± 0.023	17.681 ± 0.008	16.742 ± 0.007	15.695 ± 0.022
8	12:02:24.70	+10:49:54.7	17.237 ± 0.051	17.406 ± 0.023	17.020 ± 0.008	16.652 ± 0.007	16.324 ± 0.022
9	12:02:17.02	+10:51:45.5	20.510 ± 0.064	20.805 ± 0.030	20.216 ± 0.018	19.673 ± 0.020	18.951 ± 0.041
10	12:02:14.76	+10:52:54.6	–	21.885 ± 0.058	20.528 ± 0.019	19.617 ± 0.014	18.631 ± 0.028
11	12:02:17.10	+10:51:02.5	–	23.674 ± 0.051	22.376 ± 0.098	21.823 ± 0.092	20.947 ± 0.137
12	12:02:11.32	+10:51:11.3	21.129 ± 0.089	21.249 ± 0.034	20.810 ± 0.023	20.507 ± 0.029	20.025 ± 0.066

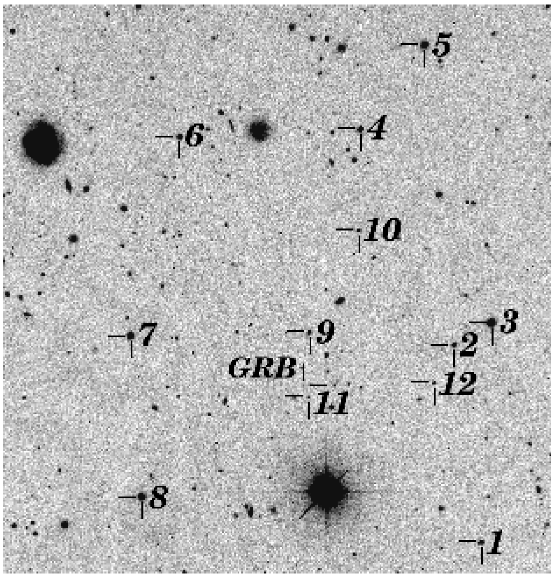

Fig. A.1. Identification chart of GRB 050408. The calibration stars and the afterglow location have been marked. The field of view is 6.0′ × 6.5′, North is to the top and East to the left.

Optical photometric calibration is based on the observation of several standard fields (Landolt 1992) using the 1.54 m Danish at La Silla (Chile) and the 1.5 m telescope at Sierra Nevada Observatory (Spain). From these observations we derive 12 secondary standards of different brightnesses in the field of the GRB. Identification of these stars is shown in Fig. A.1, while their photometric values are displayed in Table A.1.

Appendix B: Observations

In the following tables we use the *HETE-2* onset time t_0 = 2005 April 08 16:22:50.93 UT.

Table B.1. Observations in millimetre wavelengths from the Plateau du Bure interferometer (compact 6-antenna configuration on all dates). The errors are based on point-source fits in the UV plane to the phase center.

$(t - t_0)$ (days)	Band (GHz)	Flux (mJ)	3-σ limit (mJy)
3.23	86.789	0.0 ± 0.3	0.9
3.23	229.068	1.0 ± 1.6	4.8
5.19	115.477	0.5 ± 0.8	2.5
5.19	232.295	3.3 ± 1.8	5.4
10.34	86.251	0.9 ± 0.3	0.9[a]
10.34	232.171	8.4 ± 2.3	6.9[a]
11.19	108.995	–1.7 ± 1.7	5.2
11.19	228.534	–9.9 ± 6.5	19.5
12.40	108.995	–0.9 ± 0.7	2.2
12.40	228.534	3.6 ± 2.7	8.2
14.29	111.619	–0.8 ± 0.4	1.3
14.29	224.680	1.4 ± 2.1	6.3

[a] The faint detections found on this epoch are considered to be due to a statistical fluctuation or to an unusual event of interstellar scattering at high galactic latitud, taking into account the non detection the next night and the extreme spectral slope.

Table B.2. Observations in radio wavelengths from the Giant Metrewave Radio Telescope (GMRT) and Radio Astronomical Telescope Academy Nauk (RATAN-600).

$(t - t_0)$ (days)	Telescope	Band (GHz)	3-σ limit (mJy)
13.0	GMRT	1.28	0.45
13.0	RATAN-600	8.4	5.0

Table B.3. Optical observations carried out for GRB 050408. The magnitudes are in the Vega system and are not corrected for Galactic reddening.

$(t-t_0)$ (days)	Tel. + Inst.	Filter	Texp (s)	Mag	ErMag
0.4780	Dk1.54 m+DFOSC	U	9000	23.09	0.18
1.5939	4.0 mKPNO	U	1600	23.75	0.26
0.1297	6.0 mBTA+SCORPIO	B	600	22.37	0.05
0.1385	6.0 mBTA+SCORPIO	B	500	22.44	0.05
0.1467	6.0 mBTA+SCORPIO	B	600	22.46	0.05
0.1554	6.0 mBTA+SCORPIO	B	600	22.55	0.05
0.2301	6.0 mBTA+SCORPIO	B	500	22.79	0.07
0.3712	Dk1.54 m+DFOSC	B	1200	23.05	0.10
0.5681	Dk1.54 m+DFOSC	B	1200	23.54	0.17
1.5001	Dk1.54 m+DFOSC	B	9000	24.26	0.10
242.5213	3.5 mCAHA	B	1800	25.32[4]	0.22
0.2245	6.0 mBTA+SCORPIO	V	300	22.11	0.06
0.3599	Dk1.54 m+DFOSC	V	600	22.24	0.09
1.6206	4.0 mKPNO	V	1200	23.98	0.22
2.4394	4.0 mCTIO	V	1500	24.10	0.17
0.0155	Kiso 1.05 Schmidt	Rc	300	>19.50	–
0.0388	1.0 mLOT	Rc[5]	180	20.34	0.10
0.0859	1.0 mZeiss	Rc	900	20.99	0.09
0.0919	1.0 mLOT	Rc[5]	180	20.80	0.18
0.0956	1.0 mLOT	Rc[5]	300	20.98	0.14
0.1029	6.0 mBTA+SCORPIO	Rc	180	20.92	0.03
0.1068	6.0 mBTA+SCORPIO	Rc	180	20.94	0.03
0.1104	6.0 mBTA+SCORPIO	Rc	180	20.92	0.03
0.1139	6.0 mBTA+SCORPIO	Rc	180	20.92	0.02
0.1172	6.0 mBTA+SCORPIO	Rc	180	20.95	0.02
0.1207	6.0 mBTA+SCORPIO	Rc	180	21.03	0.03
0.1240	6.0 mBTA+SCORPIO	Rc	180	21.05	0.03
0.1471	RTT150+TFOSC	Rc	450	21.13	0.08
0.1629	RTT150+TFOSC	Rc	450	21.05	0.06
0.1771	RTT150+TFOSC	Rc	540	21.10	0.06
0.1863	RTT150+TFOSC	Rc	540	21.19	0.06
0.1984	RTT150+TFOSC	Rc	480	21.42	0.08

Table B.3. continued.

$(t - t_0)$ (days)	Tel. + Inst.	Filter	Texp (s)	Mag	ErMag
0.2080	RTT150+TFOSC	Rc	480	21.40	0.08
0.2175	RTT150+TFOSC	Rc	480	21.39	0.09
0.2204	6.0 mBTA+SCORPIO	Rc	180	21.32	0.04
0.2296	RTT150+TFOSC	Rc	480	21.19	0.06
0.2380	RTT150+TFOSC	Rc	480	21.52	0.09
0.2463	RTT150+TFOSC	Rc	480	21.56	0.08
0.2742	RTT150+TFOSC	Rc	720	21.52	0.06
0.2867	RTT150+TFOSC	Rc	720	21.58	0.06
0.3392	RTT150+TFOSC	Rc	600	21.80	0.12
0.3496	RTT150+TFOSC	Rc	600	21.50	0.09
0.3540	Dk1.54 m+DFOSC	Rc	300	21.81	0.13
0.3600	RTT150+TFOSC	Rc	600	21.84	0.14
0.3705	RTT150+TFOSC	Rc	600	21.95	0.15
0.4362	Dk1.54 m+DFOSC	Rc	600	21.91	0.08
0.5366	Dk1.54 m+DFOSC	Rc	900	22.00	0.07
0.5963	Dk1.54 m+DFOSC	Rc	1200	22.02	0.08
0.7166	2.0 mFTN	Rc	2400	22.50	0.11
1.4024	Dk1.54 m+DFOSC	Rc	5700	23.08	0.09
1.5864	Dk1.54 m+DFOSC	Rc	3600	23.31	0.14
2.4911	Dk1.54 m+DFOSC	Rc	14 700	23.86	0.17
3.4506	Dk1.54 m+DFOSC	Rc	14 000	23.85	0.13
5.1575	RTT150+ANDOR CCD	Rc	9000	23.70	0.20
5.5124	Dk1.54 m+DFOSC	Rc	7200	23.72	0.18
7.4663	Dk1.54 m+DFOSC	Rc	15 600	23.97	0.11
30.2567	3.5 mTNG	Rc	3600	24.64	0.17
242.4885	3.5 mCAHA	Rc	2500	24.60[4]	0.15
0.3871	Dk1.54 m+DFOSC	Ic	1200	21.25	0.07
0.6137	Dk1.54 m+DFOSC	Ic	1500	22.52	0.11
6.4766	Dk1.54 m+DFOSC	Ic	13 800	23.50	0.18
242.5446	3.5 mCAHA	Ic	1500	>24.0	–
–0.00340	WIDGET	Unfiltered	95	>9.7	–
–0.00224	WIDGET	Unfiltered	95	>9.7	–
–0.00108	WIDGET	Unfiltered	95	>9.7	–
0.00007	WIDGET	Unfiltered	95	>9.8	–
0.00123	WIDGET	Unfiltered	95	>9.7	–

[4] Host galaxy magnitude.
[5] *VR* broad band filter was transformed to *R*c.